Journal of Applied Mechanics and Technical Physics, Vol. 41, No. 5, 2000

SOME PHYSICAL PROBLEMS OF CUMULATION

Yu. A. Trishin

UDC 532.522

A review and analysis of some results related to the phenomenon of cumulation are given. The various models used to describe this phenomenon are considered.

1. Model of an Inviscid Incompressible Fluid. The hydrodynamic theory of formation of cumulative jets and their interaction with a target proposed by Lavrent'ev [1] is based on the model of an inviscid incompressible fluid. From the hydrodynamic theory of cumulation it follows that cumulative jets are formed either in oblique collision of explosively driven plates or in explosive compression of a thin conical liner in the cavity of a high explosive (HE) charge.

One of the most important results of the hydrodynamic theory of cumulation [1] was the application of the theory of jets to shaped charges. The formation of a shaped-charge jet can be described by considering the collision of two identical plane jets at angle 2α. From the hydrodynamic theory it follows that the shaped-charge jet velocity in a laboratory coordinate system is defined as the sum of the velocity of the contact point and the velocity of the impinging jet at infinity in a coordinate system in which the oblique collision pattern of the jets is stationary. Then, an actual shaped charge is a HE cylinder that has, in one end, a conical cavity lined with a thin metal layer.

The formation of a shaped charge can be described rejecting the assumption that the metal liner can have only a conical shape.

In present work, we showed that a shaped charge can be produced by placing, in a cylindrical explosive charge, a cylindrical metal tube with wall thickness increasing in the direction of detonation-wave propagation (Fig. 1). It is also possible to use a cylindrical tube with constant wall thickness placed in a conical explosive charge, where the detonation-wave front propagates from the cone base to the apex (Fig. 2). In this case, it is necessary to ensure the required collision angle, which is in the jet formation region [2], and in the plane case, where the impinging plate velocity is normal to the plates, the critical angle α_2^* is given by the expression

$$\alpha_2^* = \arctan\,(U/c_0), \tag{1.1}$$

where U is the plate velocity and c_0 is the initial velocity of sound in the plate material. Thus, in the plane $(U, 2\alpha)$, curve (1.1) divides the collision region with the jet into two regions: solid monolithic jets form above curve (1.1) and diffused jets arise below it. It is possible to use a generalized criterion of jet formation if we convert to a laboratory coordinate system. Then, if the phase velocity v_k of the point of collision of the shaped-charge liner elements on the symmetry axis is lower than the initial velocity of sound in the neighborhood of the collision, the disturbances can move forward along the liner and the collision proceeds with formation of a jet [2]. Hence, for formation of a monolithic shaped-charge jet, the following condition must be satisfied:

$$v_k \leqslant c_0. \tag{1.2}$$

Lavrent'ev Institute of Hydrodynamics, Russian Academy of Sciences, Novosibirsk 630090. Translated from Prikladnaya Mekhanika i Tekhnicheskaya Fizika, Vol. 41, No. 5, pp. 10–26, September–October, 2000. Original article submitted March 29, 2000.

0021-8944/00/4105-0773 $25.00

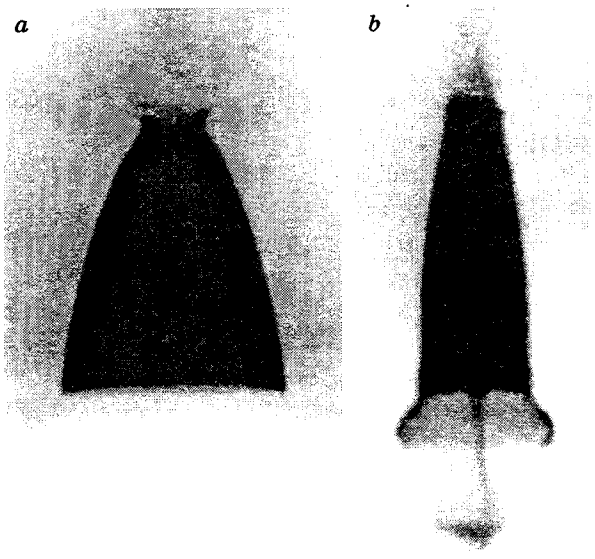

Fig. 1

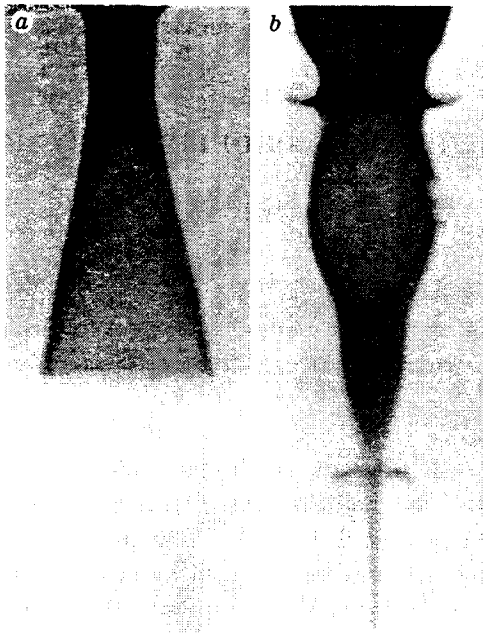

Fig. 2

Fig. 1. Flash x-ray photographs of compression of a cylindrical copper liner with increasing thickness by a detonation wave propagating along a coaxial HE charge (from top to bottom) from the thinner to the thicker layer of the liner at $t = 12.2$ (a) and 22 μsec (b).

Fig. 2. X-ray photographs of compression of a copper cylindrical liner of constant thickness by a gliding detonation wave propagating along a conical HE charge from the cone base to its apex (from top to bottom) for $t = 16.5$ (a) and 31.7 μsec (b).

Figure 2 shows an x-ray photograph of compression of a copper tube of constant thickness ($R_{10} =$ 1.43 cm and $R_0 = 1.3$ cm) 60 mm long lined with a conical layer of 50/50 TNT/RDX with a cone angle of 30°. From Fig. 2 it is evident that the upper part of the cylindrical liner exploded without formation of a shaped-charge jet since the collision angle was smaller than the angle α_2^*. The detonation propagates over the HE layer from the cone base to apex. Here the HE layer thickness changes from 19 mm at the beginning of the copper tube to 2.7 mm at the lower edge of the copper liner tube. .

Figure 3 gives an x-ray photograph of collapse of a cylindrical tube 60 mm high (the thickness of the upper part of the tube increases to the middle from 0 to 1.3 mm). It can be seen that, compared to a tube of constant thickness, the collapse angle in the upper part of the tube increases under the action of the same conical explosive layer. In this case, the velocities of the shaped-charge jet from the upper and lower parts of the tube are different. As shown in Fig. 3b, there is penetration of the jet from the upper part of the tube by the jet from its lower part, which moves with higher velocity. Therefore, in the design of a shaped charge, it is necessary that the velocity of the shaped-charge jet formed decrease continuously along the length of the tube.

Let us consider the shaped charge shown schematically in Fig. 4 [R_1 is the inner radius of the liner, R_0 is the distance along the normal from the inner surface of the liner to its intersection with the symmetry axis x, $\delta_1(x)$ is the liner wall thickness, $\delta_2(x)$ is the HE layer thickness, l is the tube length, and D is the detonation wave velocity].

We assume that the liner elements collapse independently of the neighboring sections in the direction perpendicular to the inner surface of the liner. Results of experiments confirm this assumption for cylindrical and weakly conical liners.

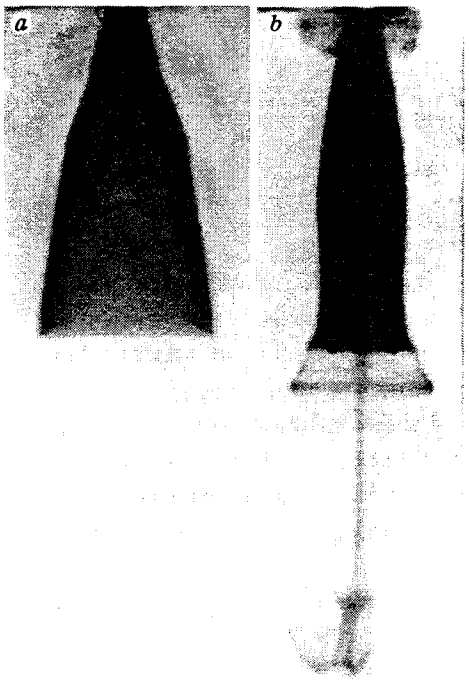

Fig. 3. X-ray photographs of compression of a cylindrical liner with variable wall thickness in the upper part of the liner by a gliding detonation wave propagating along a conical HE charge from the cone base to its apex (from top to bottom) at $t = 15.2$ (a) and 25.1 μsec (b).

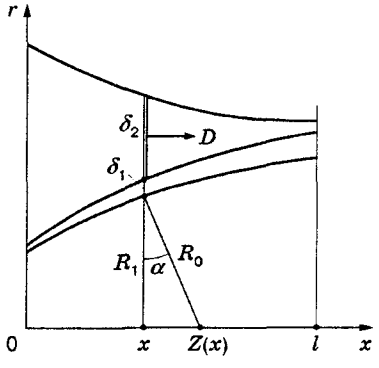

Fig. 4. Diagram of a shaped HE charge with an axisymmetric copper liner of variable thickness enclosed by an explosive layer of variable thickness.

Thus, the shaped charge is divided by cross sections into elementary incompressible cylindrical rings. From the solution of the problem of collapse of a cylindrical piston [3–5], we use two characteristics of the process — the time of collapse t_* and the velocity of the cylindrical cylinder piston U.

The coordinate of the point of contact where the liner elements belonging to the given section collapse is denoted by $Z(x)$: $Z(x) = x + R_1(x) \tan \alpha(x)$, and the time of collapse of these elements reckoned from the moment when the detonation wave reaches the top of the liner ($x = 0$) is denoted by $t(Z)$. Then,

$$t = t_D + t_* = x/D + R_0\tau_*/D,$$

where t_D is the time of arrival of the detonation wave from the cross section $x = 0$ at the cross section x, t_* is the time of collapse of the cylindrical ring in the cross section x, and τ_* is the dimensionless time of collapse

of the cylindrical ring. From these formulas it is easy to obtain the velocity of the point of contact v_k of the walls of the collapsing liner:

$$\frac{v_k}{D} = \frac{1}{D}\frac{dZ}{dt} = \frac{1}{D}\Big(1 + \frac{d(R_1 \tan\alpha)}{dx}\Big)\Big/\Big(1 + \frac{d(R_0\tau_*)}{dx}\Big).$$

For a liner with a strictly conical inner surface,

$$v_k(x) = D\Big[\Big(\tau_* \frac{dR_1}{dx} + R_1 \frac{\partial\tau_*}{\partial\delta_1}\frac{d\delta_1}{dx} + R_1 \frac{\partial\tau_*}{\partial\delta_2}\frac{d\delta_2}{dx} + \cos\alpha_0\Big)\cos\alpha_0\Big]^{-1}, \tag{1.3}$$

where $R_1 = r_0 + x\tan\alpha_0$; $\alpha(x) = \alpha_0 = \text{const}$. As noted above, to describe the jet formation process in a quasistationary approximation, it is necessary to relate the liner collapse characteristics in each cross section to the corresponding characteristics in the problems of impinging jets in a coordinate system in which the flow is steady. It is possible to determine the collapse angle $\theta(Z)$ from the condition that the velocity of the point of contact $v_k(Z)$ is the velocity of the coordinate system used to pass from the stationary jet problem of sheet flow to the problem of acceleration of this sheet along the normal to its surface. Then, considering U the velocity of normal acceleration of the liner (sheet), we have $v_k = U/\sin\theta(Z)$. When the jet formation condition $v_k < c_0$ is satisfied, the shaped-charge jet velocity is determined from the hydrodynamic theory of cumulation:

$$V_{\text{jet}} = \frac{U}{\sin\theta} + \frac{U}{\tan\theta} = v_k(z)[1 + \cos\theta(Z)], \tag{1.4}$$

and the jet radius is given by

$$r_{\text{jet}}(Z) = \sqrt{\frac{\delta_1^2 + 2\delta_1 R_0}{2}(1 - \cos\theta)}. \tag{1.5}$$

Thus, relations (1.2) and (1.3) define the condition of jet formation from a liner with a conical inner surface or, for $\alpha_0 = 0$, from a liner with a cylindrical inner surface. Relations (1.4) and (1.5) are the result of calculation of the shaped-charge jet formed.

For a cylindrical HE charge with a cylindrical liner with constant wall thickness, calculations using relation (1.3) yields $v_k = D$, but if, in addition, the necessary condition of jet formation $v_k \leqslant c_0$ is satisfied, i.e., $v_k = D \leqslant c_0$, a shaped-charge jet is also formed from a coaxial device. Figure 5 gives a flash x-ray photograph of compression of a cylindrical aluminum tube ($c_0 = 5.5$ km/sec) by a cylindrical HE charge (6ZhV ammonite and $D = 3.5$ km/sec). The photograph clearly shows the shaped-charge jet formed. These studies made it possible to design, in particular, shaped charges with a cylindrical copper inner liner with a diameter of 39 mm and a tube length of $h = 60$ mm surrounded by a 60-mm-diameter layer of 50/50 TNT/RDX, which penetrate into steel at a depth of 255 mm (4.25 diameters of the HE charge). Similar HE charges of 60 mm diameter but with a purely conical inner surface $2\alpha = 12°$ penetrate into steel at a depth of 420 mm (7 diameters of the HE charge).

2. Model of an Inviscid Compressible Fluid. As is known, a shaped-charge jet is formed from the inner layer of a shaped-charge liner, and the outer layer forms a pestle. Therefore, it is possible to design a shaped charge with a layered liner whose inner copper layer forms a shaped-charge jet and whose outer layer is made of a different metal.

Let us consider the flow pattern produced by operation of a shaped charge with a two-layer liner. A diagram of a shaped charge with a two-layer liner is presented in Fig. 6. Two close sections normal to the surface of the plates show a segment containing the liner and the HE charge. We assume that the thickness of the inner layer 1 of the liner is much smaller than that of the outer layer 2, which in turn is lower than the thickness of the HE layer.

We analyze the motion of the chosen section of the two-layer liner after arrival of a detonation wave at it. For the liner material, we consider the problem in an acoustic approximation. Then, a (p, u) diagram with center (u_0, p_0) generally has the form $p - p_0 = \pm\rho c(u - u_0)$ [6]. Upon decay of the discontinuity on the boundary cc (HE is the outer layer of the liner 2) in the layer 2 of the liner, a shock wave propagates toward the layer 1 with parameters p_* and propagation velocity c_2, where $p_* = \rho_2 c_2 u_*$ (Fig. 6). When the shock

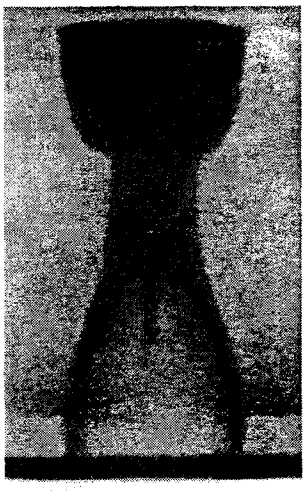

Fig. 5

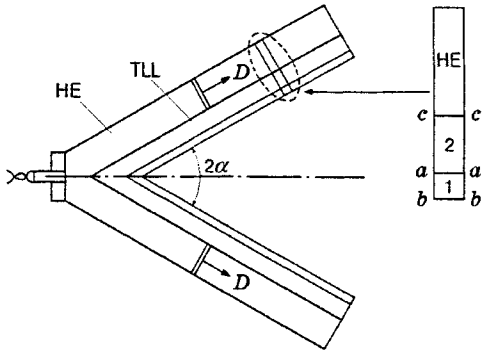

Fig. 6

Fig. 5. X-ray photograph of compression of an aluminum cylindrical liner of constant thickness by a detonation wave propagating along a coaxial explosive charge (from top to bottom) in the case where the detonation velocity (in 6ZhV ammonite) is lower than the velocity of sound in the liner material (aluminum) ($t = 26.1$ μsec).

Fig. 6. Diagram of a plane shaped charge with a two-layer liner and a segment of a HE charge with a two-layer liner (TLL) between two close cross sections perpendicular to the HE layer and the two-layer liner: 1 and 2 are the inner and outer layers of the liner, respectively.

wave reaches the interface aa, a reflected wave moves along the outer layer 2, and a rarefaction wave moves along the inner layer 1. The latter, having reached the free surface bb, is reflected from it and again interacts with the contact interface aa, etc.

We consider the case $R_1 < R_2$, where $R_i = \rho_i c_i$. In the (p, u) diagram (Fig. 7), the possible states of the materials of the liner layers 1 and 2 are the straight lines p_1 and p_2, which issue from the point O. When the shock wave (p_*, u_*) emerges from the interface aa, a wave with parameters p_a, u_a propagates on both sides of aa [(u_a, p_a) is the point A_0 of intersection of the straight line $\tilde{p}_2$, which is symmetric to the straight line p_2 about $u = u_*$, with the straight line p_1]: $\tilde{p}_2 - p_* = R_2(u_* - u)$ and $p_1 = R_1 u$. Hence for $p_* = p_1 = \tilde{p}_2$ and $u = u_*$, we obtain

$$u_a = \frac{2R_2}{R_1 + R_2} u_*, \qquad p_a = \frac{2R_1 R_2}{R_1 + R_2} u_*. \tag{2.1}$$

Next, the wave with parameters p_a and u_a reaches the free surface of the liner bb, from which a rarefaction wave departs. The latter is the point of intersection of the straight line $\tilde{p}_1$, which is symmetric to the straight line p_1 about the straight line $u = u_a$, with the straight line p_1. Thus, from the relation $\tilde{p}_1 - p_a = -R_1(u - u_a)$, taking into account relation (2.1), we obtain the mass velocity in the inner layer of the liner behind the rarefaction wave front:

$$u_1^{(1)} = 2u_a = \frac{4R_2}{R_1 + R_2} u_*. \tag{2.2}$$

The rarefaction wave, having reached the interface aa, transforms the material of the layer 2 into a state with parameters $u_2^{(1)}$ and 0 [$(u_2^{(1)}, 0)$ is the point of intersection of the straight lines $p=0$ and $\tilde{p}_2 = p_* + R_2(u_* - u)$]. Then, for $\tilde{p}_2 = 0$ and $u = u_2^{(1)}$ we obtain

$$u_2^{(1)} = p_*/R_2 + u_* = 2u_*. \tag{2.3}$$

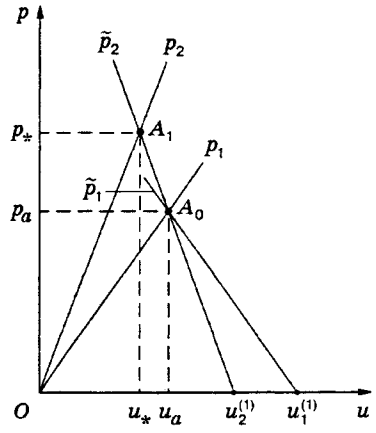

Fig. 7

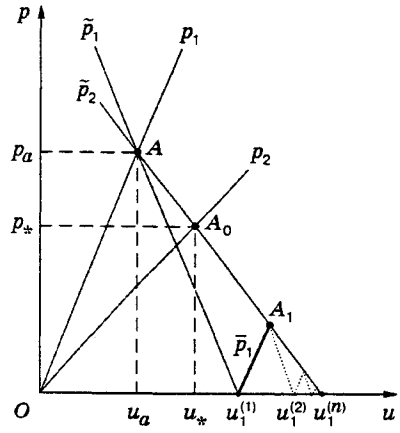

Fig. 8

Fig. 7. (p, u) diagram of the process of circulation of waves in the chosen segment (Fig. 6) in the case $R_1 < R_2$.

Fig. 8. (p, u) diagram of the process of circulation of waves in the chosen segment (Fig. 6) in the case $R_1 > R_2$.

Comparing (2.2) and (2.3) and taking into account that $R_1 < R_2$, we obtain $u_2^{(1)} < u_1^{(1)}$. This implies that during collapse, the bimetallic liner layers. The velocity and energy of the inner layer of the liner are determined by the trapped pulse.

Let us consider the case $R_1 > R_2$, where the acoustic resistance of the inner layer is higher than that of the outer layer (Fig. 8). Just as in the previous case, during interaction of the shock wave with the surface aa, from the state A_0 we obtain the state A given by relation (2.1). Next, the shock wave reaches the free liner surface bb, and the material of the layer 1 passes to the state $p = 0$, $u = u_1^{(1)}$:

$$u_1^{(1)} = p_a/R_1 + u_a = 2u_a. \tag{2.4}$$

When the rarefaction wave (2.4) reaches the surface aa, the state A_1 arises, which is the point of intersection of $\bar{p}_1$ and $\tilde{p}_2$. The following notation is introduced: $\bar{p}_i$ are straight lines parallel to p_i and $\tilde{p}_i$ are straight lines symmetric to p_i about the vertical straight lines $u = u_i$. The coordinates of the point A_1 on the (p, u) diagram are

$$u_{A1} = u_A + \frac{2R_1}{R_1 + R_2} u_A, \qquad p_{A1} = p_A - \frac{2R_1R_2}{R_1 + R_2} u_A, \tag{2.5}$$

where u_A and p_A are defined, as above, by relations (2.1). Next, the wave with parameters (2.5) reaches the free surface bb and is reflected, and behind the rarefaction wave front, the new state $u_1^{(2)}$, $p_1^{(2)} = 0$ arises:

$$u_1^{(2)} = u_1^{(1)} + \frac{2(R_1 - R_2)}{R_1 + R_2} u_A. \tag{2.6}$$

Here $u_1^{(1)}$ is given by relation (2.4). From (2.6) it follows that $u_1^{(2)} > u_1^{(1)}$ for $R_1 > R_2$, i.e., there is continuous acceleration of the material of the inner layer of the liner and pumping into it of the kinetic energy from the outer layer of the liner.

The further course of the (p, u) diagrams is shown in Fig. 8 by dotted lines. It is evident that the maximum velocity of the inner layer reaches the greatest possible velocity $u_1^{(n)}$ in the material of layer 2 (the point of intersection of the straight lines $\tilde{p}_2$ and $p = 0$): $\tilde{p}_2 - p_* = R_2(u_* - u)$, whence for $\tilde{p}_2 = 0$ and $u = u_1^{(n)}$, $u_1^{(n)}$ is defined by the formula $u_1^{(n)} = p_*/R_2 + u_* = 2u_*$, where the velocity u_* is different from that in the case $R_1 < R_2$.

Thus, the inner and outer layers of the liner collapse in contact with each other as an integral unit. This should influence the shaped-charge jet parameters: during convergence of a bimetallic liner there is additional energy cumulation in the inner layer of the liner.

Let us consider the decay of the discontinuity between the explosive and the outer layer of the liner. For the (p, u) diagram of 50/50 TNT/RDX, we have

$$p = p_H \frac{64}{27}\Big(1 - \frac{u}{D}\Big)^3 = \frac{16}{27}\rho D^2\Big(1 - \frac{u}{D}\Big)^3. \tag{2.7}$$

For cast 50/50 TNT/RDX, we have $p_H = 252$ kbar, $D = 7.65$ km/sec, $u_H = 1.9$ km/sec, and $\rho = 1.68$ g/cm^3. Then, expanding relation (2.7) in a series, with accuracy up to $O(u/D)^2$ we have

$$p = \frac{16}{27}\rho D^2\Big(1 - \frac{3u}{D}\Big). \tag{2.8}$$

Therefore, for the point of intersection of the (p, u) diagrams for the HE (2.8) and the material of the outer layer of the liner with parameters ρ_2 and c_2, we obtain the expressions

$$u_* = \frac{16}{27} D\Big(\frac{16}{9} + \frac{\rho_2 c_2}{\rho D}\Big)^{-1}, \qquad p_* = \rho_2 c_2 u_*. \tag{2.9}$$

For a continuous copper liner ($\rho_2 = 8.9$ g/cm^3 and $c_2 = 4$ km/sec) in contact with 50/50 TNT/RDX, from relation (2.9) we obtain $u_* = 0.95$ km/sec and $p_* = 340$ kbar. Therefore, the velocity of acceleration of the copper liner is ultimately equal to $u_1^{(1)} = 2u_* = 1.92$ km/sec. For a two-layer liner with an aluminum outer layer ($\rho_2 = 2.7$ g/cm^3 and $c_2 = 5.5$ km/sec) and a copper inner layer ($\rho_1 = 8.9$ g/cm^3 and $c_1 = 4$ km/sec), the inner layer gains a velocity twice as high as the initial velocity of the aluminum layer $u_* = 1.49$ km/sec, i.e., a velocity of $u_n^{(1)} = 2u_* = 2.98$ km/sec.

Figures 9 and 10 give flash x-ray photographs of collapse and jet formation for a two-layer (Al–Cu) liner and a three-layer (Plexiglas–Al–Cu) liner. The normal flow of the copper jet formed is evident. The shaped-charge jet penetration is the same for the two-layer (Al–Cu) liner and a solid copper liner of the same weight. For the two-layer liner, the shaped-charge jet parameters are much more stable than those for a homogeneous copper liner. It is shown experimentally that if the copper jet and the copper pestle inside the aluminum pestle have identical radii, the shaped-charge jet flow is stable. If the thickness of the copper pestle is smaller than the jet thickness, the shaped-charge jet flow becomes unstable and the penetration into a steel target decreases sharply.

3. Real Model of a Newtonian Viscous Fluid. The main difference in the operation of plane shaped charges and charges with axisymmetric liners is that an explosively driven wedge-shaped liner is not subjected to considerable deformation. An axisymmetric liner compressed by the HE detonation products undergoes large deformations, under which the liner layers slide over each other. In this case, the energy-dissipation mechanisms have a significant effect on the convergence of the liner to the symmetry axis. For explosively driven charges with plane liners, energy dissipation is practically absent even for acceleration by a gliding detonation wave because there is no sliding of the plate layers. This is suggested by the shape of the indicator wires pressed in the plate [7]. After oblique collision of the plates, the shape of the wires is considerably distorted, especially near the collision surface. Hence, only at the stage of collision and jet formation is dissipation of mechanical energy possible in plane charges.

For explosive compression of cylindrical liners, it has been shown experimentally and theoretically [8] that the convergence of the liner to the symmetry axis is described most adequately by the model of a Newtonian fluid. Hence, because of the action of viscous forces during collapse of axisymmetric liners, the energy-dissipation process should change the characteristics of the shaped-charge jets formed depending on the type of liner material. In addition, it is possible to choose charge and cylindrical-liner parameters such that the initial kinetic energy of the liner is completely converted to thermal energy and the liner stops upon reaching a certain radius R^* [8].

The heating due to viscosity is nonuniform over the liner thickness and increases in the process of convergence of the liner to the center. Maximum increase in temperature is attained on its inner surface.

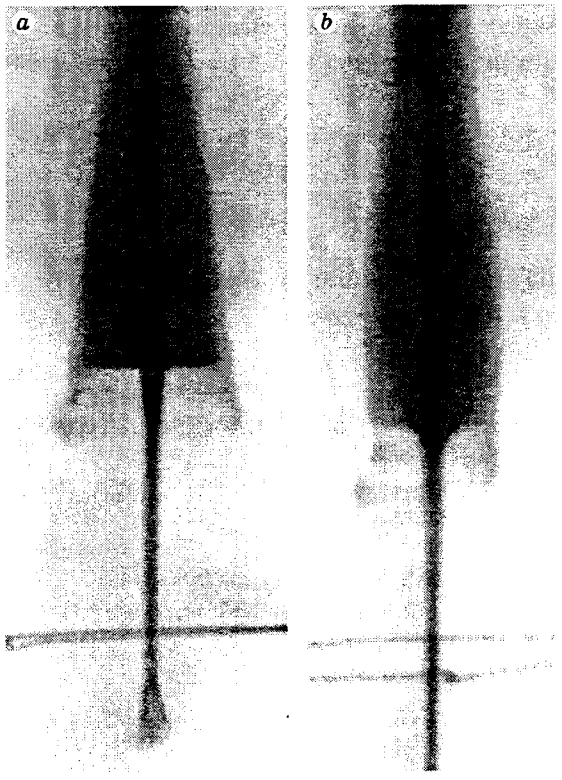

Fig. 9

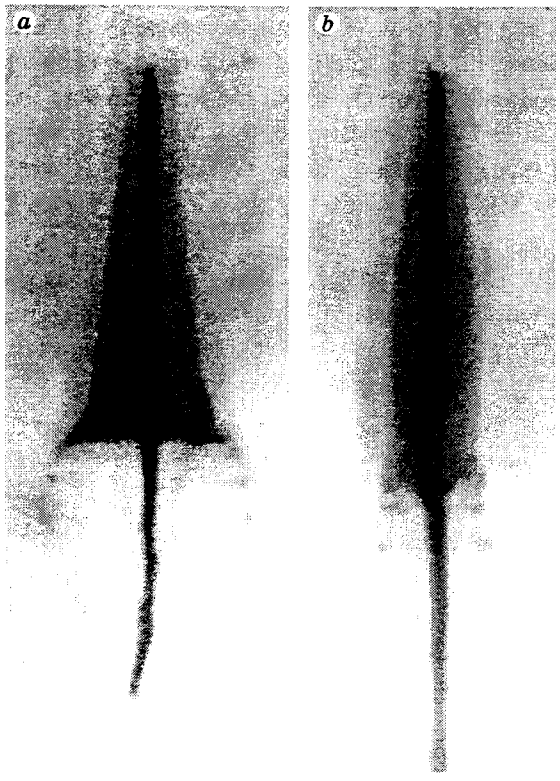

Fig. 10

Fig. 9. Flash x-ray photographs of collapse and jet formation for a conical two-layer liner (the outer layer of the liner is aluminum and the inner layer is copper) for $t = 28$ (a) and 33 μsec (b).

Fig. 10. Flash x-ray photographs of collapse and jet formation for a conical three-layer liner (the outer layer of the liner is made of Plexiglass, the middle layer is aluminum, and the inner layer is copper) for $t = 27$ (a) and 37 μsec (b).

The increase in temperature changes the properties of the liner material and, in particular, the dynamic viscosity [9].

According to the Frenkel–Eyring theory [10], which was developed for liquids and used by Mineev and Savinov [11] to describe experiments on shock-wave loading of metals up to the melting point, the dynamic viscosity η of a liquid depends on the temperature T and degree of compression σ as follows:

$$\eta(\sigma, T) = \eta_0 \sigma \exp\left[E_a(\sigma)/T\right].$$

From physical considerations it follows that for the work related to viscous motion during formation of vacancies, the activation energy E_a has the form $E_a = A + B\sigma^3$. The constants A and B were determined from shock-wave experiments for metals.

For aluminum and lead, Mineev and Savinov [11] established experimentally that with increase in the shock-wave intensity the viscosity initially increases, and then, passing through the maximum at $\sigma \approx 1.4$, decreases. The nontrivial dependence of the viscosity coefficient on the shock-wave intensity can apparently be explained qualitatively by competition of the processes involved in the compression of the material and thermal processes.

A similar situation is observed for convergence of a cylindrical liner to the axis. The decrease in the viscosity of the inner layers due to their stronger heating is compensated for by the higher degree of compression since on the inner surface of the cylinder and in the adjacent layers, the pressure increases with decrease in the liner convergence radius.

Martynyuk [12] showed that at heating times of 0.1–10.0 μsec, a metallic liquid can be overheated up to the ultimately stable states determined by the spinodal. Under real conditions, overheating of liquids is hindered because of the presence of ready centers (for example, gas inclusions). However, with high power energy input, the fraction of the material evaporated through the free surface and the surface of the nuclei is insignificant. In this case, there may be overheating of the liquid and close approach to the spinodal, which is the boundary of thermodynamic stability of the metastable liquid that corresponds to the liquid–vapor transition. Estimates show that nearly ultimate overheating of the metastable liquid is possible at $\dot{T} \geqslant 10^8$ K/sec [12].

As a metastable liquid approaches the spinodal, fluctuations increase sharply. With intersection of the spinodal there is loss of thermodynamic stability of the liquid phase, and, as a result of explosion, the liquid enters a two-phase state.

Thus, for cylindrical or weakly conical convergence of a liner material to the axis, a phase explosion is also possible. The x-ray photograph presented in [9, Fig. 2] shows a copper tube ($R_{10} = 1$ cm, $R_0 = 0.9$ cm, and $\dot{R}_0 \approx 1$ km/sec) compressed by a 50/50 TNT/RDX layer in the gliding detonation regime. Inside the tube, one can clearly see separate liquid fragments of the inner layers of the liner that formed after explosion of these layers.

To determine the effect of the physicomechanical properties of liner materials on the characteristics of the jets formed, we performed a series of experiments using flash radiography. In the experiments, we used a charge of 50/50 TNT/RDX whose bottom contained a shaped-charge liner of various metals [9]. In the experiments, the cone angle was varied ($2\alpha = 30$, 45, and 60°). The liner material consists of various grades of steels (St. 3, St. 20, and 30KhGSA) and M1 copper. The densities of these metals are approximately identical, which ensures constant kinematic characteristics of shaped charges with various liner materials.

The experiments showed that steel jets break up into separate fragments, while copper jets continue to stretch at the same moments without visible rupture. The elongation and breakup of a steel jet is accompanied by its softening and not by the "line formation" typical of a copper jet with large elongation. Therefore, the penetration of steel jets into targets is always smaller than that for copper jets. At a distance of 150 mm from a steel plate, the penetration is equal to 195 mm for a copper jet and 110 mm for a steel jet. It should be noted that the breakup of a steel jet begins within 20–25 μsec after arrival of the detonation wave at the conical liner apex and does not depend on the cone angle in the examined range of angles $2\alpha = 30$–60°.

Thus, during operation of a shaped charge with axisymmetric liners, overheating of the liner material is possible. This can lead to a strong phase explosion of the inner layers even at the stage of liner compression by the HE detonation products or a weak phase "explosion," resulting in softening of the material at the stage of formation and motion of the shaped-charge jet.

4. Model of a Porous Medium. Previous studies have shown that by varying the initial porosity, it is possible to control the physicomechanical properties of shaped-charge liner materials during liner acceleration by a HE charge. It was found that, depending on the initial porosity, there may be two different shaped-charge jet flows — jet flows that fill the entire shaped-charge cavity and normal shaped-charge jets capable of penetrating into metal targets [13, 14]. The first type of jet flows can be used to apply coatings from shaped-charge liner materials (shaped-charge deposition) [15] and to design new materials using phase transitions and physicochemical transformations [16]. The second type of flows with monolithic jets allows one to extend the range of materials used in practical cumulation, by using tungsten liners in shaped charges, and to increase the penetration into targets for charges with porous liners compared to shaped charges with monolithic liners of the same geometry.

The idea underlying the design of a shaped charge with a porous metallic liner is that in liner compression by HE detonation products, a porous liner material is heated more strongly than the same liner of the same monolithic material. The degree of heating is determined by the porosity of the liner $m = \rho_0/\rho_{00}$ (ρ_0 and ρ_{00} are the densities of the solid and porous materials). As the temperature increases during liner acceleration by a HE charge, the viscosity of the liner decreases strongly. This allows one to describe the

collapse process without energy losses in dissipative processes, in the same manner as is done in the model of an inviscid fluid. Choosing the initial liner porosity m in such a manner that the liner is heated to a temperature at which the viscosity decreases considerably, we obtain a liner with the same density as the monolithic liner but with much lower viscosity [14].

At the same time, a shaped-charge liner material can be preheated by an external source, for example, joule heat. As was shown by experiments [14], the shaped-charge jet velocity in this case becomes equal to the jet velocity calculated from the hydrodynamic theory of cumulation [1], which is based on the model of an inviscid incompressible fluid. Hence, preheating of the liner material transforms it to an inviscid medium, and this considerably reduces dissipative losses during explosive compression of the shaped-charge liner and formation of a shaped-charge jet.

To describe the behavior of a porous liner in a shock wave, we use the Zababakhin–Zel'dovich shock adiabat [17]:

$$p_H = \frac{(h-1)p_x - 2E_x/V}{h - V_{00}/V} = \frac{(h-1)p_x - 2E_x/V}{h - mV_0/V}, \qquad h = \frac{2}{\Gamma} + 1,$$

where the elastic pressure component p_x is taken in the form of the Tait equation $p_x = B[(V_0/V)^n - 1]$ (n and B are parameters of the material). Assuming that $V_0/V = 1 + \varepsilon$, where $\varepsilon \ll 1$, we obtain $p_x = nB\varepsilon$, and, for the shock adiabat,

$$p_H = \frac{2nB}{2 - (m-1)\Gamma}\,\varepsilon = \alpha_0 \varepsilon, \tag{4.1}$$

where Γ is the Grüneisen factor.

After arrival of the shock-wave at the free surface of the liner, the material is expanded isentropically in the rarefaction wave. The isentropic lines $p_S(V)$ and $E_S(V)$ can be calculated from the Mie–Grüneisen equation

$$E_S - E_H = V(p_S - p_H)/\Gamma, \tag{4.2}$$

where E_H and p_H are the specific internal energy and pressure on the hugoniot adiabat. From relations (4.1), (4.2), and $E_H = p_H(V_{00} - V)/2$ and $p_S(V) = -dE_S(V)/dV$, we obtain the differential equation

$$\frac{dp_S}{dV} + \frac{\Gamma+1}{V}\,p_S = \frac{\Gamma+2}{2V}\,p_H + \Big(\frac{\Gamma+2}{2} - \frac{m\Gamma}{2}\,\frac{V_0}{V}\Big)\frac{dp_H}{dV},$$

which, in view of the smallness of $\varepsilon = V_0/V - 1$, becomes the equation

$$\frac{dp_S}{d\varepsilon} - (\Gamma+1)(1-\varepsilon)p_S = \beta\{2 - (m-1)\Gamma - [2 + (m+1)\Gamma]\varepsilon\}, \tag{4.3}$$

where $\beta = nB/(2 - (m-1)\Gamma)$. For $\Gamma = \text{const}$, its solution is

$$\pi_S = \frac{p_S}{\rho_0 c_0^2} = \frac{\pi_* - \varepsilon_*}{1 + (1+\Gamma)\varepsilon_*} + \frac{1 + (1+\Gamma)\pi_*}{1 + (1+\Gamma)\varepsilon_*}\,\varepsilon. \tag{4.4}$$

Here the integration constant is determined from the condition $p_S = p_H = p_*$ for $V = V_*$ ($\varepsilon = \varepsilon_*$).

The degree of expansion of the liner material in the rarefaction wave is obtained from (4.4) under the assumption that $\pi_S = 0$:

$$\varepsilon_{0k} = -\frac{\pi_* - \varepsilon_*}{1 + (\Gamma+1)\pi_*}. \tag{4.5}$$

The velocity of sound behind the shock-wave front $c_H^2 = dp_H/d\rho$ is determined from (4.1):

$$c_H = c_0\sqrt{\frac{2}{2 - (m-1)\Gamma}}. \tag{4.6}$$

After unloading of the material to $p_S = 0$ in the rarefaction wave, from (4.4) it follows that the velocity of sound $c_S^2 = dp_S/d\rho$ becomes equal to

TABLE 1

ε	$m = 1.2$, $c_H/c_0 = 1.12$			$m = 1.5$, $c_H/c_0 = 1.41$			$m = 2.1$, $c_H/c_0 = 3.16$			$m = 2.5$, $c_H/c_0 = 1.41$		
	π	$\lvert\varepsilon_{0k}\rvert$	c_S/c_0	π	$\lvert\varepsilon_{0k}\rvert$	c_S/c_0	π	$\lvert\varepsilon_{0k}\rvert$	c_S/c_0	π	$\lvert\varepsilon_{0k}\rvert$	c_S/c_0
0.01	0.013	0.020	1.004	0.02	0.009	1.02	0.01	0.085	1.158	0.02	0.028	1.05
0.05	0.063	0.011	1.015	0.10	0.038	1.06	0.50	0.220	1.715	0.10	0.115	1.24
0.07	0.088	0.014	1.020	0.14	0.049	1.08	0.70	0.248	1.980	0.14	0.148	1.34
0.10	0.125	0.018	1.030	0.20	0.063	1.11	1.10	0.275	2.390	0.20	0.186	1.51
0.15	0.188	0.024	1.040	0.30	0.079	1.15	1.50	0.300	3.162	0.30	0.237	1.86
0.20	0.250	0.029	1.050	0.40	0.091	1.17	2.00	0.314	4.183	0.40	0.273	2.345

TABLE 2

ε	$m = 1.2$			$m = 1.5$			$m = 2.1$			$m = 2.5$		
	π	ΔT_H	ΔT_S	π	ΔT_H	ΔT_S	π	ΔT_H	ΔT_S	π	ΔT_H	ΔT_S
0.01	0.013	51	50	0.02	200	197	0.1	2185	2030	0.02	600	597
0.05	0.063	260	240	0.10	1050	930	0.5	10550	8840	0.10	2900	2770
0.07	0.088	375	330	0.14	1500	1270	0.7	14500	12005	0.14	4020	3800
0.10	0.125	550	460	0.20	2210	1755	1.0	20070	16560	0.20	5640	5300
0.15	0.188	865	660	0.30	3460	2530	1.5	28600	24080	0.30	8090	7570
0.20	0.250	1200	860	0.40	4820	3280	2.0	36130	31570	0.40	10440	9850

$$c_S = c_0\sqrt{\frac{1+(1+\Gamma)\pi_*}{1+(1+\Gamma)\varepsilon_*}}. \tag{4.7}$$

The calculation results for porous copper with a normal course of the shock adiabats p_H ($m < 2/\Gamma + 1$) and an abnormal course ($m > 2/\Gamma + 1$) are given in Table 1. The columns $m = 1.2$ and $m = 1.5$ correspond to the normal course of shock adiabats and the columns $m = 2.1$ and $m = 2.5$ correspond to the abnormal course.

Table 2 gives the heating temperatures for porous copper liners in a shock wave $\Delta T_H = (E_H - E_x)/c$, where c is the specific heat of copper. The Hugoniot adiabat for porous materials has the form

$$E_H = \frac{p_H}{2}(V_{00} - V) = \frac{p_H V}{2}\left(m\frac{V_0}{V} - 1\right) = \frac{p_H V_0}{2}(m - 1 + \varepsilon).$$

Substituting the value of p_H from relation (4.1) into this equality, we obtain

$$E_H = \frac{nBV_0}{2-(m-1)\Gamma}(m-1+\varepsilon)\varepsilon = \frac{c_0^2}{2-(m-1)\Gamma}(m-1+\varepsilon)\varepsilon. \tag{4.8}$$

For $m = 1$, from (4.8) we obtain an expression for the internal specific energy of monolithic material E_H^c, which coincides with the expression for the energy of cold compression $E_H^c = E_x = c_0^2\varepsilon^2/2$ with accuracy up to ε^3. Table 2 also gives the residual temperatures ΔT_S after isentropic unloading in the rarefaction wave to zero pressure:

$$\Delta T_S = \left(E_H - \int_{V_*}^{V_{0k}} p_S\,dV\right)\Big/c.$$

From Tables 1 and 2 it follows that with increase in the porosity m, the temperatures T_H and T_S, $|\varepsilon_{0k}|$ [see (4.5)], and the velocity of sound behind the rarefaction-wave front c_S [see (4.7)] increase if the shock-wave pressure π_* is the same for different values of the porosity. For the normal course of the shock adiabats, $\alpha_0 > 0$ and $\varepsilon > 0$ in formula (4.1), and for the abnormal course, $\alpha_0 < 0$ and $\varepsilon < 0$, and, hence, $p_H > 0$.

We note that for the abnormal shock adiabats, the velocity of sound c_S in the rarefaction wave tends to infinity ($c_S \to \infty$) (4.7) at $\varepsilon_* = -1/(\Gamma + 1)$ [for a copper liner ($\Gamma = 2$), $\varepsilon_* = -0.333$]. Thus it is necessary that the pressure in copper in the shock wave be equal to

$$\pi_* = |\alpha|\,|\varepsilon_*| = 2/\{(\Gamma+1)[(m-1)\Gamma-1]\}$$

($\pi_* = 2/3$; $p_H \simeq 950$ kbar for porosity $m = 2.5$ and $p_H \simeq 474$ kbar for $m = 3$).

When examining the decay of discontinuity on the boundary between the porous liner and the explosive material, we consider the behavior of (p, u) diagrams. It is known that the internal specific energy of condensed material in a shock wave is equal to the specific kinetic energy $E_H = u^2/2$. Hence, we obtain the equation of the (p, u)-diagram for the shock wave $p_H V_0(m - 1 + \varepsilon) = u^2$. Substituting the values of p_H from (4.4) into this equation, we obtain $p^2 + \alpha_0(m-1)p - \alpha_0\rho_0 u^2 = 0$. For the abnormal course of the shock adiabat, the (p, u) diagrams for $V_0/V = 1 - \varepsilon$ have the form $pV_0(m - 1 - \varepsilon) = u^2$, which leads to the quadratic equation $p^2 - |\alpha_0|(m-1)p + |\alpha_0|\rho_0 u^2 = 0$. When the shock wave arrives at the free liner surface, a rarefaction wave goes to the depth of the liner and the liner is imparted the additional velocity

$$u_{\max} = \int_{V_*}^{V_{0k}} \sqrt{-dV\Big/dp_S}.$$

From this, substituting the value of the differential dp_S from relation (4.4), we obtain

$$u = \int_{V_*}^{V} \sqrt{\frac{1+(\Gamma+1)\pi_*}{1+(\Gamma+1)\varepsilon_*}\,\frac{c_0^2}{V^2}\,(dV)^2} = c_0\sqrt{\frac{1+(\Gamma+1)\pi_*}{1+(\Gamma+1)\varepsilon_*}}\int_{V_*}^{V}\frac{dV}{V}$$

or

$$u = c_S \ln\frac{V}{V_*} = c_S \ln\Big(\frac{V}{V_0}\,\frac{V_0}{V_*}\Big) = c_S\Big(\ln\frac{V_0}{V_*} - \ln\frac{V_0}{V}\Big).$$

Substituting the values $V_0/V_* = 1 + \varepsilon_*$ and $V_0/V = 1 + \varepsilon$ into the last expression, we have $u = c_S(\varepsilon_* - \varepsilon)$. Replacing ε by its value from relation (4.4), we obtain

$$u = c_S\varepsilon_* - c_S\,\frac{\pi_S - \{(\pi_* - \varepsilon_*)/[1+(\Gamma+1)\varepsilon_*]\}}{c_S^2/c_0^2}.$$

Hence we obtain the (p, u) diagram of the rarefaction wave:

$$\pi_S = \pi_* - \sqrt{\frac{1+(\Gamma+1)\pi_*}{1+(\Gamma+1)\varepsilon_*}}\,\frac{u}{c_0} = \pi_* - \frac{c_S}{c_0}v. \tag{4.9}$$

The maximum additional velocity of the medium in the rarefaction wave is attained during unloading to $\pi_S = 0$ ($(V = V_{0k})$: $v_{\max} = c_0\pi_*/c_S$, where $\pi_* = \alpha\varepsilon_* = 2\varepsilon_*/(2 - (m-1)\Gamma)$.

In the rarefaction wave with the abnormal course of shock adiabats ($m > 2/\Gamma + 1$), ε_* in formula (4.9) is negative and π_* is positive. From Table 1 it follows that with increase in the porosity, the velocity of sound c_S also increases. This circumstance was used in the experiment to produce a monolithic shaped-charge jet from a cylindrical liner surrounded by a cylindrical HE layer. According to the jet formation criterion (1.2), a shaped-charge jet is formed when the contact point has subsonic velocity. In a telescopic charge, the velocity of the contact point is equal to the HE detonation velocity. Therefore, for a bulk RDX charge ($D = 6.2$ km/sec) with a monolithic cylindrical nickel liner ($c_0 = 4.6$ km/sec), a jet is not formed. When a porous nickel liner is used ($m = 2.2$), a jet is formed since the velocity of sound c_S increases with increase in the porosity, as observed in experiments.

For shaped charges with porous conical liners (Fig. 11), powders of nickel, copper, and iron were used, and the explosive charge was RDX of bulk density ($\rho = 1\text{g/cm}^3$ and $D = 6.2$ km/sec). Conical liners with specified porosity were produced by pressing on a static press.

The experiments performed with charges having porous liners showed that the jet flow pattern is basically preserved but there are differences. For a nickel powder of bulk density ($\rho_{00} = 3.2$ g/cm^3), a standard jet flow — a shaped-charge jet and a pestle — is formed but there is breakup of the jet due to the softening of the jet material. For liners with higher porosity, for example, of copper with bulk density

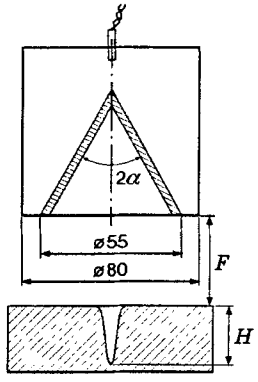

Fig. 11. Diagram of a shaped charge with a porous conical liner.

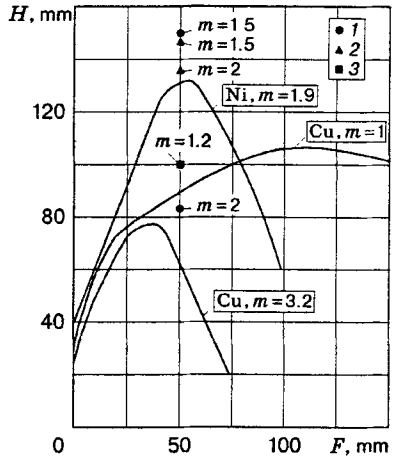

Fig. 12. Experimental curve of penetration into a steel target versus the distance from the lower end of the shaped charge to the target for conical liners made of various materials and having various porosities: 1) copper (Cu); 2) nickel (Ni); 3) iron (Fe).

(ρ_{00} = 1.8 g/cm^3 and m = 4.9), a jet is not formed. Just after the beginning of liner collapse, a cloud of particles is observed, which flies in the direction of the symmetry axis and fills the entire cavity of the shaped charge. These experiments suggest that there is an optimal focal distance, as for shaped charges with liners of the monolithic material follows. In addition, there is a large difference in penetration for liners of bulk density and pressed liners. The penetration into a steel target increases with decrease in the porosity, and for a certain value of the porosity, it reaches a maximum value.

The experimental curve of the penetration into a steel target versus the focal distance for a shaped charge 80-mm high with a monolithic copper liner ($2\alpha = 60°$) of the same design (Fig. 11) is shown in Fig. 12. The results of experiments for porous nickel and copper liners (solid curves) are also given here. Dots show the penetrations into a steel target for shaped charges with bulk RDX versus the distance F = 50 mm: for copper (Cu), the penetration H = 84 mm at m = 2 and H = 150 mm at m = 1.5, for nickel (Ni), H = 135 mm at m = 2 and H = 150 mm at m = 1.5, and for iron (Fe), H = 100 at m = 1.2. Each of the indicated values of H is averaged over 3 or 4 experiments, and the spread does not exceed 10 mm. It should be noted that a solid copper liner charge (m = 1) having the same weight as a charge with a porous liner penetrates a steel target to a depth not exceeding H = 115 mm (Fig. 12).

The same charges with porous liners of tungsten with bulk density (m = 1.8) produce compact shaped-charge jets.

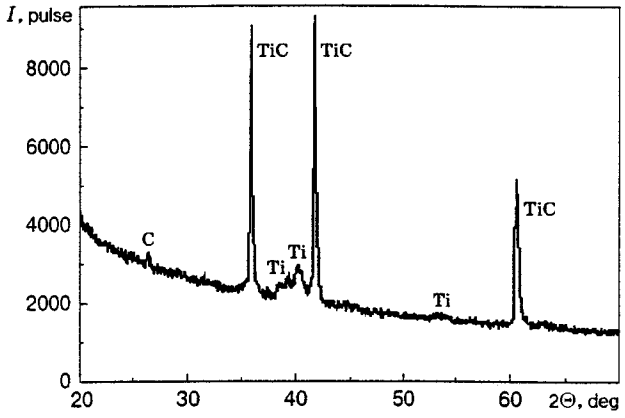

Fig. 13. Diffraction pattern of the layer produced by application of a mechanical mixture of Ti and C in a shaped-charge liner on a titanium substrate.

5. Physicochemical Transformation of Shaped Charges during Application of Coatings on Substrates. For charges with highly porous liners, when the heating temperature of the liner in the shock wave exceeds the spinodal temperature, there is a phase explosion of the liner material. This results in formation of a vapor–liquid cloud, which fills the entire internal space of the shaped-charge liner and propagates along the symmetry axis of the liner.

At a heating temperature of the liner below the spinodal temperature, there may be a weak phase "explosion" of the metastable liquid, where the material can evaporate both through the free surface and the surface of heterogeneous nuclei. When a weak phase "explosion" occurs in the jet material, time is required for a vapor–liquid cloud to form from the shaped-charge liner material. Therefore, application of coatings using shaped charges with porous liners [15, 16, 18] is performed from a rather large distance from the substrate. For ignition, the charges were at 400–500 mm from the substrate target on which the coating was applied.

In the experiments with coatings, we used axisymmetric shaped charges with conical liners of constant wall thickness. The liners were made of mechanical mixtures of powders of tungsten or titanium with carbon (flaky graphite or soot) or nitrogen (granular carbamide), which were poured in a conical gap between walls made of thin cardboard; the liner wall thickness (the width of the gap) was approximately 3 mm. A cylindrical HE charge was made of RDX of bulk density, and the diameter and height of the charge were 80 mm (see Fig. 11).

X-ray diffraction studies of the applied coating materials were performed on a DRON-3M apparatus (R = 192; CuK radiation, nickel filter, and scintillation detector with amplitude discrimination) for angles 2Θ = 5–70° with a rate of variation of the angle of 1 deg/min. The samples were 26-mm-diameter spacers fixed in a standard brass ring.

The experiments performed showed that when a mechanical mixture Ti and C is applied on various metallic substrates (titanium and steel), titanium is almost entirely converted to titanium carbide TiC, and the coating layer is rather thick and continuous since diffraction lines from the substrate are practically absent in the diffraction pattern (Fig. 13). Similar results are obtained for the application of coatings from a mechanical mixture of Ti with granular carbamide (the mixture was prepared in a 1 : 1 proportion by volume): titanium practically entirely reacts with nitrogen, forming a film of crystalline titanium nitride.

A more complicated case is the layers formed by application of a mechanical mixture of W and C. A comparison of experimental results with results of analysis of the phase diagram of the W–C system yielded an estimate of the temperature region equivalent to static conditions. Using this estimate, it is established that a decrease in the shaped-charge liner cone angle is accompanied by an increase in the pressure and, probably, temperature of the shaped-charge jet. In particular, an analysis of diffraction patterns of the layers produced by liners with $2\alpha = 90°$ showed that tungsten carbides are not present in the coatings. For liner

cone angle $2\alpha = 75°$, the applied coating contains, along with metallic tungsten, the β phase of W_2C, and with decrease in the angle to 60°, the amount of this phase increases. In this case, the diffraction pattern shows lines of the α phase of WC. At an angle of 45° and a temperature higher than 2875°, the β phase of WC forms and its lines are clearly seen in the diffraction pattern. The temperature range of existence of this phase lies between the ranges of existence of W_2C and α-phase WC.

From the results obtained it follows that new phases with unique properties can be produced by changing shaped-charge characteristics.

REFERENCES

1. M. A. Lavrent'ev, "Shaped charge and the principles of its work," *Usp. Mat. Nauk*, **12**, No. 4, 41–52 (1957).
2. S. A. Kinelovskii and Yu. A. Trishin, "Physical aspects of cumulation," *Fiz. Goreniya Vzryva*, **16**, No. 5, 26–40 (1980).
3. S. A. Kinelovskii, N. I. Matyushkin, and Yu. A. Trishin, "Convergence of an incompressible ring to the center under the action of detonation products," in: *Dynamics of Continuous Media* (collected scientific papers) [in Russian], Vol. 5, Novosibirsk (1970), pp. 23–32.
4. S. A. Kinelovskii, N. I. Matyushkin, and Yu. A. Trishin, "Motion of a cylindrical cylinder piston to the center," in: *Dynamics of Continuous Media* (collected scientific papers) [in Russian], Vol. 7, Novosibirsk (1971), pp. 105–114.
5. S. A. Kinelovskii, N. I. Matyushkin, and Yu. A. Trishin, "Motion of a cylindrical piston surrounded by a layer of expanding gas," *ibid.*, pp. 115–124.
6. V. I. Laptev and Yu. A. Trishin, "Increase in the initial velocity and pressure under impact on an inhomogeneous target," *Prikl. Mekh. Tekh. Fiz.*, No. 6, 128–132 (1974).
7. V. I. Lpatev, M. V. Rubtsov, and Yu. A. Trishin, "Use of the model of a viscous fluid to describe high-velocity jet flows of metals," *Fiz. Goreniya Vzryva*, **20**, No. 1, 80–86 (1984).
8. N. I. Matyushkin and Yu. A. Trishin, "Some effects that arise in explosive compression of a viscous cylindrical liner," *Prikl. Mekh. Tekh. Fiz.*, No. 3, 99–112 (1978).
9. Yu. A. Trishin, "Effect of energy dissipation on the shaped-charge flow regime," *Prikl. Mekh. Tekh. Fiz.*, **41**, No. 4, 3–11 (2000).
10. Ya. I. Frenkel', *Introduction to the Theory of Metals* [in Russian], Fizmatgiz, Moscow (1958).
11. V. N. Mineev and E. V. Śavinov, "Viscosity and melting point of aluminum, lead, and sodium chloride under shock compression," *Zh. Éksp. Teor. Fiz.*, **52**, No. 3, 629–636 (1967).
12. M. M. Martynyuk "Phase explosion of a metastable liquid," *Fiz. Goreniya Vzryva*, **13**, No. 2, 213–229 (1977).
13. V. G. Kabulashvili and Y. A. Trishin, "Jet flows in explosive compression of porous liners and their applications," in: *Inform. Bull.*, Inst. of Hydrodynamics, Sib. Div., Russian Acad. of Sci., **18**, 149–157 (1988).
14. Yu. A. Trishin, "Effect of energy dissipation on the shaped-charge flow regime," in: Proc. IV Int. Conf. *Zababakhin Scientific Readings* (Snezhinsk, October 1995, Inst. of Tech. Phys.), Snezhinsk (1996), pp. 23–30.
15. V. G. Kabulashvili, S. A. Kinelovskii, Yu. N. Popov, and Yu. A. Trishin, USSR Inventor's Certificate 1729035, SU 1729035 A 1, "Device for applying coatings," Applied 12.22.91; Publ. 1992, Bull. No. 15.
16. S. A. Gromilov, S. A. Kinelovskii, Yu. N. Popov, and Yu. A. Trishin, "Possibility of physicochemical transformations in applying coatings using shaped charges," *Fiz. Goreniya Vzryva*, **33**, No. 6, 127–130 (1997).
17. Ya. B. Zel'dovich and Yu. P. Raizer, *Physics of Shock Waves and High-Temperature Hydrodynamic Phenomena*, Academic Press, New York (1967).
18. S. A. Gromilov, S. A. Kinelovskii, Yu. N. Popov, and Yu. A. Trishin, Russian Federation Patent No. 2137709 RU, 6 C 01 In 31/30, 21/06. "Method of producing 'metal–light nonmetal' compounds," *Otkr. Izobr.*, No. 26. (1999).